Sub-system fault tolerance with the Bacon-Shor code

Panos Aliferis ¹ and Andrew W. Cross ^{2,3}

Institute for Quantum Information, California Institute of Technology, Pasadena, CA 91125
 Massachusetts Institute of Technology, 77 Massachusetts Avenue, Cambridge, MA 02139
 IBM Research Division, T. J. Watson Research Center, P. O. Box 218, Yorktown Heights, NY 10598 (Dated: February 9, 2020)

We discuss how the presence of gauge sub-systems in the Bacon-Shor code [D. Bacon, *Phys. Rev.* A **73**, 012340 (2006)] leads to remarkably simple and efficient methods for fault-tolerant error correction (FTEC). Most notably, FTEC does not require entangled ancillary states and it can be implemented with nearest-neighbor two-qubit measurements. By using these methods, we prove a lower bound on the quantum accuracy threshold, 1.94×10^{-4} for adversarial stochastic noise, that improves previous lower bounds by nearly an order of magnitude.

PACS numbers: 03.67.Pp

Operating a full-scale quantum computer will require methods for protecting against decoherence or systematic hardware imperfections. Understanding physical noise and developing schemes of computation that limit its effects has been the subject of the theory of fault-tolerant quantum computation [1]. One of the central results of this theory, the quantum threshold theorem, shows that any ideal quantum computation can be efficiently simulated to any desired accuracy by a noisy quantum computer provided that noise is *local* and its strength is below a certain critical value known as the quantum accuracy threshold [2]. Apart from the theoretical importance of proving the existence of an accuracy threshold for a given noise model, the actual value of the accuracy threshold is of great practical interest as it represents the desired target accuracy of prospective implementations of quantum computation. In this paper, we follow this second line of research and we present methods of fault-tolerant quantum computation based on a new sub-system code which significantly improve both the value of the accuracy threshold and the overhead associated with encoded computation.

Sub-system codes protect quantum information from noise by mapping the system to be encoded (e.g., one logical qubit) into a *sub-system* of a larger system [3, 4]; in fact, such a mapping provides the most general possible encoding once we require that the evolution and measurement statistics are identical for the encoded system and the encoding sub-system [5]. In more detail, if we let \mathcal{H}_S be the Hilbert space of the system to be encoded, the encoding map identifies density operators and observables in \mathcal{H}_S with density states and observables in a sub-system with Hilbert space \mathcal{H}_L which lies inside a larger Hilbert space \mathcal{H} , $\mathcal{H} = (\mathcal{H}_L \otimes \mathcal{H}_T) \oplus \mathcal{H}_R$, where \mathcal{H}_T describes additional "gauge" sub-systems not necessarily protected by noise and \mathcal{H}_R labels the "rest" of \mathcal{H} . Fault-tolerant quantum computation has traditionally used sub-space codes that can be seen as sub-system codes where \mathcal{H}_T is one-dimensional encoding no sub-system.

Interestingly, the converse is also true: For any sub-

system code there exists a corresponding sub-space code that can be obtained by "picking a gauge," i.e., by projecting the state in \mathcal{H}_T onto a pure state [4]. Because of this connection, sub-system codes do not have properties that make them fundamentally different from sub-space codes. Nevertheless, as has been discussed in the literature for the case of noiseless operations, sub-system codes are in a certain sense more efficient than the corresponding sub-space codes since they require the extraction of fewer syndrome bits [6, 7] (but, see also [8]). By focusing on one particular example of a code, we will next see that sub-system codes are also advantageous when we consider noisy operations. But, the reason is different: Now, the advantage comes from the simplicity of the quantum circuits that implement fault-tolerant error correction, whose complexity is an important determining factor for both the accuracy threshold and the overhead.

We will consider fault-tolerant quantum circuits where computation is encoded using a sub-system code due to Bacon [7]—because of the close relation of this code with Shor's code [9], we will refer to it as the Bacon-Shor code. There is a different Bacon-Shor code for every integer n > 1; for fixed n, the corresponding code, $C_{BS}^{(n)}$, is a distance-n stabilizer CSS code [10] encoding one protected logical qubit into a code block of n^2 physical qubits.

It is convenient to place the n^2 qubits in the $\mathcal{C}_{BS}^{(n)}$ block on the *vertices* of a $n \times n$ square lattice; see Fig. 1. Then, the code is defined in terms of its stabilizer group \mathcal{S} [10] that is generated by

$$S = \langle X_{\text{row}-j,\text{row}-(j+1)}; Z_{\text{col}-j,\text{col}-(j+1)} | j \in \mathbb{Z}_{n-1} \rangle, (1)$$

where we have used the short-hand notation for the Pauli matrices $X \equiv \sigma_{\rm x}, \ Z \equiv \sigma_{\rm z}$, and $X_{{\rm row}-j,{\rm row}-(j+1)}$ (resp. $Z_{{\rm col}-j}Z_{{\rm col}-(j+1)}$) denotes a tensor product of X (resp. Z) operators acting on all qubits in rows (resp. columns) j and j+1.

The code $syndrome\ \vec{e}$ —i.e., the binary vector of eigenvalues of the 2(n-1) stabilizer generators in Eq. (1)—induces a decomposition of the Hilbert space \mathcal{H} of the

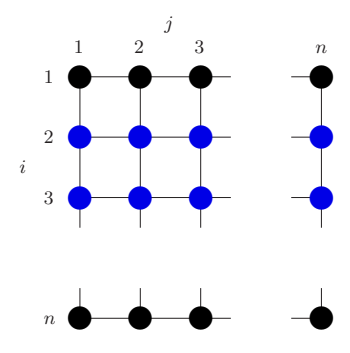


FIG. 1: (color online) Qubits in the $C_{BS}^{(n)}$ block sit on the vertices of a $n \times n$ square lattice. One element of the code stabilizer is shown: $X_{\text{row}-2,\text{row}-3}$ applies X on all qubits shown in blue

 n^2 qubits in the code block into sub-spaces encoding $n^2-2(n-1)=(n-1)^2+1$ logical qubits. Therefore, within each sub-space with fixed syndrome—and, in particular, within the $code\ space$ corresponding to the trivial syndrome—we can define a sub-system decomposition

$$\mathcal{H} = \bigoplus_{\vec{s}} \left(\mathcal{H}_L \otimes \mathcal{H}_T \right) , \qquad (2)$$

where we associate \mathcal{H}_L with the one logical qubit protected by the full distance n of the code. The logical Pauli operators for this logical qubit can be defined as $X_L = X_{\text{row}-1}$ (i.e., a tensor product of X operators applied on all qubits in the first row) and $Z_L = Z_{\text{col}-1}$ (i.e., a tensor product of Z operators applied on all qubits in the first column). We associate \mathcal{H}_T with the remaining $(n-1)^2$ logical qubits whose logical Pauli operators can be chosen from the non-abelian group

$$T = \langle X_{j,i} X_{j+1,i} ; Z_{i,j} Z_{i,j+1} | i \in \mathbb{Z}_n ; j \in \mathbb{Z}_{n-1} \rangle$$
, (3)

where we have used the notation $O_{i,j}$ for an operator O acting on the qubit with coordinates (i,j). Indeed, the operators in T commute with the stabilizer generators in Eq. (1), commute with the logical operators X_L and Z_L and, furthermore, can be grouped into $(n-1)^2$ independent pairs of anti-commuting operators, with operators in different pairs commuting.

Given some non-trivial syndrome value, error recovery for the logical qubit encoded in \mathcal{H}_L proceeds in a similar manner as in the classical repetition code: The eigenvalues of the stabilizer generators $\{X_{\text{row}-i,\text{row}-(i+1)}\}$ can be used to correct Z errors on up to $\lfloor n/2 \rfloor$ rows. Moreover, only the parity of Z errors in each row is relevant: an operator acting as Z on a pair of qubits at the same row is an operator in T and, therefore, has no effect on the protected information in \mathcal{H}_L . Error recovery for X errors proceeds similarly along the columns. Further intuition on the Bacon-Shor code can be obtained by considering its derivation from known sub-space codes; see Section A in the Appendix.

Since the logical Pauli operators for the logical qubits encoded in \mathcal{H}_T act non-trivially on only two qubits in the code block, if we take into consideration all $(n-1)^2 + 1$ logical qubits, then $\mathcal{C}_{BS}^{(n)}$ is a distance-2 code. It is therefore error detecting but not, in general, error correcting. However, if we only consider the logical qubit encoded in \mathcal{H}_L , then we effectively obtain a distance-n code and errors with support on up to $\lfloor n/2 \rfloor$ qubits in the code block can be corrected—we will call this logical qubit the protected qubit. In fact, error recovery for the protected qubit may unavoidably result in applying at the same time non-trivial logical operations with support in \mathcal{H}_T . This is not a problem as long as we never encode useful information in \mathcal{H}_T . We can think of the $(n-1)^2$ logical qubits encoded in \mathcal{H}_T as gauge qubits since they correspond to degrees of freedom for the logical information encoded in \mathcal{H}_L . In some cases it will be sufficient to disregard them. More interestingly, we will next discuss how the presence of gauge qubits leads to especially simple and efficient methods for fault-tolerant error correction.

To see how the gauge qubits can be used to our advantage, let us first explain how we can extract the code syndrome indirectly by manipulating their state. We note that we can express each stabilizer generator in Eq. (1) as

$$X_{\text{row}-j,\text{row}-(j+1)} = \bigotimes_{k=1}^{n} (X_{j,k} X_{j+1,k}) ;$$

$$Z_{\text{col}-j,\text{col}-(j+1)} = \bigotimes_{k=1}^{n} (Z_{k,j} Z_{k,j+1}) .$$
(4)

What is remarkable about this decomposition is that the operators in parentheses are supported on \mathcal{H}_T ; hence, they commute with all stabilizer generators and also commute with the logical operators for the protected qubit. Because of this, we can measure each of them separately and then Eq. (4) implies that the code syndrome can be computed by taking the appropriate parities of the measurement outcomes. Moreover, since these operators act non-trivially on only two qubits in the code block, measuring each one of them is especially easy; e.g., Fig. 2 shows simple circuits for measuring $X_{j,k}X_{j+1,k}$ and $Z_{k,j}Z_{k,j+1}$ using one ancillary qubit.

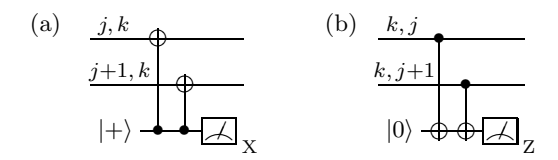


FIG. 2: (a) A circuit for measuring the operator $X_{j,k}X_{j+1,k}$ using one ancillary qubit. (b) A similar circuit for measuring $Z_{k,j}Z_{k,j+1}$. $|+\rangle \propto |0\rangle + |1\rangle$ is the +1 eigenstate of X.

This indirect method for inferring the code syndrome significantly reduces the overhead for fault-tolerant error correction (FTEC). This is because, unlike in standard FTEC methods [2], this method does not require preparing and verifying entangled ancillary states—ancillary

qubits in the $|0\rangle$ or $|+\rangle$ state are sufficient as in Fig. 2. Furthermore, for maximum qubit efficiency, a *single* ancillary qubit can be used to sequentially measure all two-qubit operators necessary to extract the syndrome! In addition, the specific two-qubit operators to be measured can be chosen to have support on neighboring qubits in the code block when these qubits are arranged on a two-dimensional lattice. For this reason, this FTEC method is especially advantageous for geometrically local architectures as those envisioned for ion-trap or solid-state implementations. Section B in the Appendix gives more details on this method and discusses its application to a two-dimensional setting.

In settings without geometric locality constraints for the interaction of qubits or when qubit movement has error rate much lower than quantum gates, other standard FTEC methods will yield the best accuracy thresholds. Since $C_{BS}^{(n)}$ is a CSS code, Steane's FTEC method [11] can be used to extract the syndrome provided we can fault-tolerantly prepare logical $|0\rangle$ ($|0\rangle_L$) and logical $|+\rangle$ ($|+\rangle_L$) states for the protected qubit. Alternatively, Knill's FTEC method [12] requires fault-tolerantly preparing two code blocks where the two protected qubits are encoded in a logical Bell state ($|\Phi_0\rangle_L \propto |0\rangle_L |0\rangle_L + |1\rangle_L |1\rangle_L$).

As is evident from the decomposition in Eq. (2), the distinctive feature of sub-system codes is that logical states in \mathcal{H}_L are not uniquely encoded: after having specified a logical state in \mathcal{H}_L , the state in \mathcal{H}_T can still be arbitrary. This freedom in choosing the state of the gauge qubits can be used to our advantage in the design of encoding circuits of logical states for the protected qubits. In particular, we will next discuss how, by exploiting this freedom, we can design remarkably simple encoding circuits for the logical ancillary states required for Steane's and Knill's FTEC methods, thus also reducing the overhead associated with the post-encoding verification of these states.

For concreteness, consider designing an encoding circuit for $|0\rangle_L$, i.e., a state in the code space which is the +1 eigenstate of Z_L . With the state in \mathcal{H}_L specified, we can choose the state in \mathcal{H}_T to be the +1 eigenstate of the gauge-qubit operators $\{X_{i,j}X_{i+1,j}\}$. In other words, our encoding circuit prepares the +1 eigenstate of the operators in the following stabilizer group:

$$S(|0\rangle_L) = \langle X_{i,j} X_{i+1,j} ; Z_{\text{col}-j} \mid i \in \mathbb{Z}_{n-1}; j \in \mathbb{Z}_n \rangle . \quad (5)$$

We recognize the state described by Eq. (5) as a tensor product of n Schrödinger "cat" states in the Hadamard-rotated basis, each one lying across a column in Fig. 1.

We can obtain the state $|+\rangle_L$ by applying a logical Hadamard transformation to the state $|0\rangle_L$. We observe that applying Hadamard gates *bitwise* has the same effect as a logical Hadamard gate up to a 90-degree rotation of the square lattice in Fig. 1 (and, also, up to a non-trivial operation acting on the gauge qubits). We can therefore

obtain $|+\rangle_L$ by first preparing $|0\rangle_L$, applying Hadamard gates bitwise and, finally, rotating the lattice in Fig. 1 by 90 degrees. The bitwise Hadamard gates will transform the Hadamard-rotated cat states to become usual cat states in the computation basis. And then, rotating the lattice by 90 degrees will align the n cat states each to lie across a row—this is our construction for $|+\rangle_L$. In addition, the logical Bell states used in Knill's FTEC method can be constructed by interacting two blocks encoded in the states $|+\rangle_L$ and $|0\rangle_L$ via a logical CNOT gate (the logical CNOT gate can be implemented by transversal CNOT gates). Section C in the Appendix gives further details on Steane's and Knill's FTEC methods and Section E presents explicit quantum circuits.

We have already discussed how to implement the logical CNOT and Hadamard gates. Universal quantum computation can be realized by including the logical phase gate $S \equiv \exp(-i\frac{\pi}{4}\sigma_z)$ and the logical Toffoli gate in our gate set; the details of achieving encoded quantum universality are discussed in Section D in the Appendix.

We have analysed the accuracy of fault-tolerant quantum circuit simulations using the concatenated $C_{BS}^{(n)}$ for various values of n. In our analysis, we have considered adversarial stochastic noise [13], i.e., the stochastic form of local noise [13, 14]. In this noise model, we assume that any r specific elementary physical operations, or "locations," in the noisy quantum circuit (single-qubit preparations, quantum gates, memory steps or singlequbit measurements) fail with probability at most ε^r for some constant $0 \le \varepsilon \le 1$. Noise is adversarial because faults need not be independent and, moreover, the noise channel acting at each faulty location can be arbitrary in general, noise acts jointly across all different faulty locations. Adversarial stochastic noise is the natural form of noise to consider when analyzing fault-tolerant circuit simulations that use concatenated codes. This is because, even if the physical noise model does not include adversarial correlations between different faulty locations, the effective noise that acts on all concatenation levels higher than the first one may include such correlations which arise due to coding and the propagation of syndrome information [13].

Our threshold lower bounds for adversarial stochastic noise were obtained by performing an analysis of malignant sets of locations on extended rectangles according to the method that was introduced in [13]. Table I summarizes our results. We carried out the required combinatorial analysis for the concatenated $\mathcal{C}_{BS}^{(3)}$ using both Steane's and Knill's FTEC methods and for the concatenated $\mathcal{C}_{BS}^{(5)}$ using only the former method due to time limitations. The analysis was done by using a computer program running for several months on a cluster of 20 Pentium III processors. Our best rigorous lower bound on the accuracy threshold, 1.94×10^{-4} , was obtained for the concatenated $\mathcal{C}_{BS}^{(5)}$. This lower bound improves by

Code Steane [[7,1,3]] $C_{BS}^{(3)}$ [[9,1,3]] $C_{BS}^{(5)}$ [[25,1,5]] Golay [[23,1,7]] $C_{BS}^{(7)}$ [[49,1,7]]	FTEC Steane Steane Knill Steane Knill Steane Steane	locs. 575 297 297 1,185 1,185 7,551 2,681	$\begin{bmatrix} \varepsilon_0 \left(\times 10^{-4} \right) \\ 0.27 \\ 1.21 \\ 1.26 \\ \textbf{1.94} \end{bmatrix}$	$\begin{array}{c} \varepsilon_0^{\rm MC} \left(\times 10^{-4}\right) \\ 1.21 \pm 0.06 \\ 1.26 \pm 0.05 \\ 1.92 \pm 0.02 \\ \textbf{2.07} \pm \textbf{0.03} \\ \approx 1 \\ 1.74 \pm 0.01 \end{array}$
$C_{BS}^{(i)}$ [[49,1,7]]	Steane Knill	2,681 $2,681$		1.74 ± 0.01 1.91 ± 0.01

TABLE I: Rigorous lower bounds on the accuracy threshold with the concatenated Bacon-Shor code of varying block size and comparison with prior rigorous lower bounds using the concatenated Steane [[7,1,3]] code [13] and Golay [[23,1,7]] code [Reichardt, Ouyang; unpublished]. The third column gives the number of locations in the CNOT extended rectangle [13]. The forth column gives exact lower bounds on the threshold ε_0 for adversarial stochastic noise; the results are obtained using a computer-assisted combinatorial analysis. The fifth column is the Monte-Carlo estimate for ε_0 with 1σ uncertainties. Bold fonts indicate the best results in each column.

nearly an order of magnitude the 2.73×10^{-5} lower bound that was proved in [13] with the concatenated Steane [[7,1,3]] code.

Analyzing codes of larger block size than $C_{BS}^{(5)}$ proved to be computationally difficult in this exact setting. In these cases, we have used a Monte-Carlo method: We uniformly sample the set of fault paths with a fixed number of faulty locations inside an extended rectangle and we estimate what fraction \hat{f} of these sets is malignant as defined in [13]. This, in turn, gives estimates of the exact combinatorial coefficients with a $\underline{\operatorname{standard}\ \operatorname{er}} \mathrm{ror}$ that can be determined by using $\sigma_{\hat{f}} = \sqrt{\hat{f}(1-\hat{f})/N}$ where N is the sample size. Given these estimates, we can then obtain a lower bound on the accuracy threshold as in the exact case. We have also applied this Monte-Carlo method to the cases where we could extract the exact combinatorics in order to provide evidence that the Monte-Carlo estimates are accurate. Indeed, as can be seen in Table I. the exact threshold lower bounds in those cases lie within 1σ of the estimated lower bounds. Our Monte-Carlo results for the variety of codes we have analysed give evidence that the accuracy threshold achieves a maximum of $(2.07\pm0.03)\times10^{-4}$ for the Bacon-Shor code with n=5using Knill's FTEC method. Section E in the Appendix discusses the details of our threshold analysis.

In conclusion, we have shown how the presence of gauge qubits in the Bacon-Shor code can be exploited to design quantum circuits for fault-tolerant error correction with remarkable properties. We have presented a new method for fault-tolerant error correction that uses nearest-neighbor two-qubit measurements and does not require the preparation of entangled ancillary states. We expect this method to be advantageous in implementations that impose geometric locality constraints in the

interactions between qubits such as, e.g., in proposed ion-trap or solid-state schemes of quantum computation. On the other hand, standard methods for fault-tolerant error correction can be implemented using especially simple encoding circuits for the required ancillary logical states, thus greatly reducing the overhead associated with the verification of these states. Our lower bound on the quantum accuracy threshold, 1.94×10^{-4} for adversarial stochastic noise, is the best that has been rigorously proven so far and improves previous rigorous lower bounds by nearly an order of magnitude.

We are grateful to Ike Chuang, David DiVincenzo, Debbie Leung, John Preskill, Krysta Svore, and Barbara Terhal for helpful discussions and suggestions. AC thanks John Preskill for the invitation to the Caltech Institute for Quantum Information, where some of this work was done. PA is supported by the NSF under grant no. PHY-0456720. AC is partially supported by a research internship at IBM T. J. Watson Research Center.

- [1] P. Shor. In *Proc.* 37th Annual Symposium on Foundations of Computer Science, page 56, Los Alamitos, CA (1996). IEEE Computer Society Press. arXive e-print quant-ph/9605011.
- [2] see [13] and references therein.
- [3] E. Knill, R. Laflamme, and L. Viola. *Phys. Rev. Lett.* 84, 2525–2528 (2000). arXive e-print quant-ph/9908066.
- [4] D. W. Kribs, R. Laflamme, D. Poulin, and M. Lesosky. Quantum Inf. Comp. 6(4), 382–399 (2006). arXive e-print quant-ph/0504189.
- [5] E. Knill. Phys. Rev. A 74, 042301 (2006). arXive e-print quant-ph/0603252.
- [6] D. Poulin. *Phys. Rev. Lett.* **95**, 230504 (2005). arXive e-print quant-ph/0508131.
- [7] D. Bacon. Phys. Rev. A 73, 012340 (2006). arXive e-print quant-ph/0506023.
- [8] S. A. Aly, A. Klappenecker, and P. K. Sarvepalli. arXive e-print quant-ph/0610153.
- [9] P. Shor. Phys. Rev. A **52**, 2493–2496(R) (1995).
- [10] D. Gottesman. Ph.D. thesis, California Institute of Technology, Pasadena, CA (1997). arXive e-print quant-ph/9705052.
- [11] A. Steane. Phys. Rev. Lett. 78, 2252 (1997). arXive e-print quant-ph/9611027.
- [12] E. Knill. Nature 434, 39–44 (2005). arXive e-print quant-ph/0410199.
- [13] P. Aliferis, D. Gottesman, and J. Preskill. Quantum Inf. Comp. 6(2), 97–165 (2006). arXive e-print quant-ph/0504218.
- [14] B. M. Terhal and G. Burkard. Phys. Rev. A 71, 012336 (2005). arXive e-print quant-ph/0402104.

A. DERIVING THE BACON-SHOR CODE

Starting from Shor's code

One natural way to derive the distance-n Bacon-Shor code $(\mathcal{C}_{BS}^{(n)})$ is by starting with Shor's distance-n code $(\mathcal{C}_{Shor}^{(n)})$ as was explained for the special case n=3 in [6]. Let us call $\mathcal{C}_Z^{(n)}$ the classical n-bit repetition code mapping the logical computation-basis state $|k\rangle$ to $|k\rangle^{\otimes n} \equiv |\bar{k}\rangle$ for k=0,1. The Hadamard-rotated n-bit repetition code, $\mathcal{C}_X^{(n)}$, maps the logical states $|\pm\rangle$ to $|\pm\rangle^{\otimes n}$, where $|\pm\rangle$ denote the ± 1 eigenstates of X. Then, $\mathcal{C}_{Shor}^{(n)}$ is the concatenated $\mathcal{C}_Z^{(n)} \circ \mathcal{C}_X^{(n)}$ mapping the logical state $|k\rangle$ to $|\bar{+}\rangle^{\otimes n} + (-1)^k |\bar{-}\rangle^{\otimes n}$, where $|\pm\rangle \propto |0\rangle^{\otimes n} \pm |1\rangle^{\otimes n}$.

If we place the n^2 qubits in the $C_{Shor}^{(n)}$ block on the *vertices* of the $n \times n$ square lattice in Fig. 1, then the code's stabilizer group is generated by

$$S(C_{Shor}^{(n)}) = \langle X_{\text{row}-i,\text{row}-(i+1)}; \\ Z_{i,j}Z_{i,j+1}; Z_{n,j}Z_{n,j+1} \mid i, j \in \mathbb{Z}_{n-1} \rangle.$$
 (6)

The stabilizer in Eq. (6) fixes a two-dimensional subspace, the *code space*, encoding one logical qubit. The logical Pauli X and Z operators are respectively $X_{\text{row}-1}$ and $Z_{\text{col}-1}$.

By its construction, Shor's code treats X and Z errors asymmetrically: In each of the n rows, up to $\lfloor n/2 \rfloor X$ errors can be corrected because of the underlying classical repetition code. The code can also correct up to $\lfloor n/2 \rfloor Z$ errors on different rows—pairs of Z operators in the same row act trivially; the code is degenerate. As a first step towards removing this asymmetry, we observe that pairs of X operators in the same column commute with Z_L . It would therefore be sufficient for successful error correction if we could restore zero parity for X errors in each given column instead of correcting X errors in each row separately.

Since only the parity of X errors in each column is relevant, we can replace the n stabilizer generators $Z_{i,j}Z_{i,j+1}$ for $i \in \mathbb{Z}_n$ and fixed j by their tensor-product $Z_{\text{col}-j,\text{col}-(j+1)}$. Repeating for all $j \in \mathbb{Z}_n$, we reduce the stabilizer group of $\mathcal{C}_{Shor}^{(n)}$ in Eq. (6) to the stabilizer group of $\mathcal{C}_{BS}^{(n)}$ in Eq. (1).

Starting from Bravyi and Kitaev's surface code

We will also give an alternative derivation of $C_{BS}^{(n)}$ starting from Bravyi and Kitaev's distance-n surface code $(C_{BK}^{(n)})$ [A1]. If we place the $n^2+(n-1)^2$ qubits in the $C_{BK}^{(n)}$ block on the *edges* of a square lattice as shown in Fig. 3, the code's stabilizer group is generated by X operators acting on all qubits neighboring a vertex (*site* operators)

and Z operators acting on all qubits neighboring a vertex of the dual lattice (plaquette operators). The logical Pauli X and Z operators are respectively $X_L = X_{\text{row}-1}$ and $Z_L = Z_{\text{col}-1}$. It can easily be verified that, if all qubits with half-integer coordinates are measured in the computation basis, the remaining qubits are in the +1 eigenstate of the stabilizer generators in Eq. (1). Moreover, the logical X and Z operators have no support on the measured qubits and match the logical operators for $\mathcal{C}_{BS}^{(n)}$. This implies that the same logical state which was encoded in the $\mathcal{C}_{BK}^{(n)}$ block is, after the measurements, encoded in the protected qubit of $\mathcal{C}_{BS}^{(n)}$.

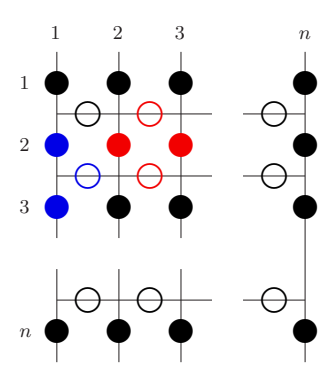


FIG. 3: (color online) Qubits in the $\mathcal{C}_{BK}^{(n)}$ block sit on the edges of a square lattice with different boundary conditions at top-bottom (rough edges) and left-right (smooth edges). Two elements of the code stabilizer are shown: X is applied on qubits shown in blue (site operator); Z is applied on qubits shown in red (plaquette operator). If all qubits shown as empty circles are measured in the computation basis, the remaining qubits will be encoded in $\mathcal{C}_{BS}^{(n)}$.

B. FTEC WITH MEASUREMENTS ON THE GAUGE QUBITS

In Fig. 2(a) (reproduced in Fig. 4(a)) we showed a circuit for implementing the measurement of the operator $X_{j,k}X_{j+1,k}$ using one ancillary qubit. An alternative circuit for implementing the same measurement in smaller depth with respect to the data gubits is shown in Fig. 4(b). Let us now explain why the two circuits in Fig. 4 are fault tolerant: In Fig. 4(a), a fault in the $|+\rangle$ state can only propagate to flip the measurement outcome but cannot harm the data. In Fig. 4(b), a fault in the sub-circuit that prepares the ancillary Bell state can always be attributed to one of the two qubits—since $\forall 2 \times 2 \text{ matrix } O, (O \otimes I) | \Phi_0 \rangle = (I \otimes O^T) | \Phi_0 \rangle$ —and, hence, an error can only propagate to at most one qubit in the data. Consider now faults in the CNOT gates acting on the data. In Fig. 4(b), the gates are transversal so errors cannot spread from one data qubit to the other. In Fig. 4(a), we might worry that there is a problem if the first CNOT is faulty because an X error can result in both

data qubits. But we soon realize that $X_{j,k}X_{j+1,k}$ is not an error—it is exactly the operator we are trying to measure and so acts trivially after the measurement has taken place.

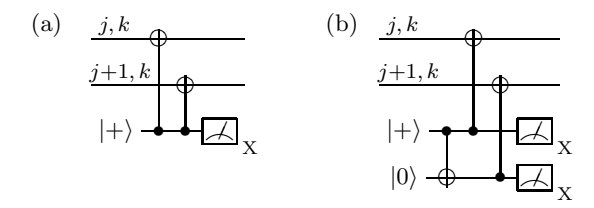


FIG. 4: (a) A circuit for measuring the operator $X_{j,k}X_{j+1,k}$ in depth two using one ancillary qubit. (b) A circuit for implementing the same measurement in depth one using an ancillary Bell state. (Depth is measured with respect to the data qubits as ancillae can be prepared separately in order to be available exactly when needed.)

We should emphasize that, just as in the standard syndrome-measurement procedure that uses cat states [1, A2], the syndrome we obtain by using circuits as in Fig. 4 cannot in general be trusted unless some of the measurements are repeated. This redundancy is necessary since a single fault can cause errors in both the data block and the measurement outcomes. Overall, we need to check that the full FTEC circuit satisfies properties 0 and 1 in §9 in [13]—this is what we mean by saying that an error-correction circuit is fault tolerant. We will return to this point when we discuss specific examples in Section E in this Appendix.

A two-dimensional layout

Fig. 5 shows a simple example of a square-lattice architecture where the qubits in the $\mathcal{C}_{BS}^{(3)}$ block are interspersed with ancillary qubits in a way that syndrome measurement can be implemented with nearest-neighbor interactions and only three qubit swaps. In the first round of FTEC, nine two-qubit ZZ operators are measured: Using superscripts to denote the data qubit acted by an operator, ancilla 1 in Fig. 5(b) is used to measure $Z^{(1)}Z^{(2)}$, ancilla 2 to measure $Z^{(1)}Z^{(3)}$ and ancilla 3 to measure $Z^{(1)}Z^{(2)}$ again (repetition of this measurement is necessary in order for the FTEC circuit to be fault tolerant in the sense defined above). At the same time, similar measurements are performed on the other two rows. Next, the three qubit swaps indicated by ellipses in Fig. 5(b) are performed which result in interchanging the qubits in rows and columns. Finally, to complete the syndrome extraction, nine two-qubit XX operators are measured by coupling data and ancillary qubits as for the first round of measurements. In this paper, we have not carried out a threshold analysis in the geometrically local setting.

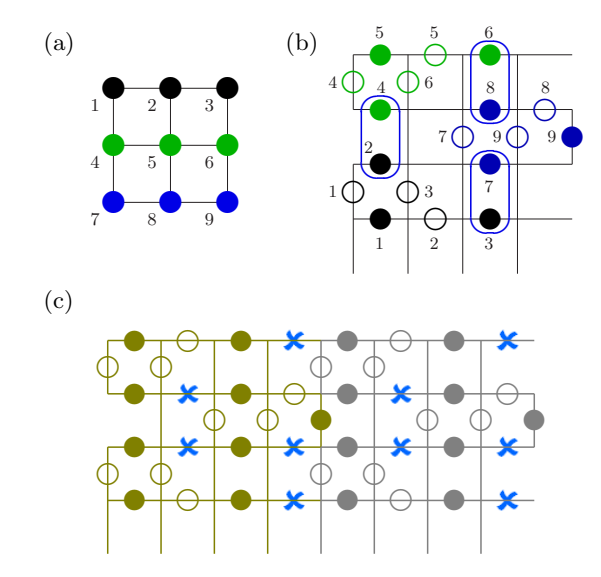


FIG. 5: (color online) (a) A color code for the qubits in the $\mathcal{C}_{BS}^{(3)}$ block. (b) The block qubits are arranged on a square lattice interspersed with nine ancillary qubits shown as empty circles. The first round of FTEC consists of nearest-neighbor gates between data and ancillary qubits of the same color followed by measurements of the ancillae. Then, after the three qubit swap operations indicated by ellipses are performed, a similar sequence of nearest-neighbor gates and measurements is performed to complete the syndrome extraction. (c) Two $\mathcal{C}_{BS}^{(3)}$ blocks side by side; e.g., these would be two of the nine sub-blocks within a code block at the second coding level when $\mathcal{C}_{BS}^{(3)}$ is concatenated with itself. Sympathetic cooling ions, which may by needed for trapped-ion implementations, may be placed at the blue 'x' positions since these positions are not used during FTEC.

C. FTEC USING ENCODED ANCILLAE

Steane's FTEC method

Recall that Steane's FTEC method [11], which applies to CSS codes, is based on the circuits

$$|\psi\rangle_L \xrightarrow{|\psi\rangle_L} ; \qquad |\psi\rangle_L \xrightarrow{|\psi\rangle_L} ; \qquad |+\rangle_L \xrightarrow{|\psi\rangle_L} ;$$

where $|\psi\rangle_L$ is the state of the input code block and $|0\rangle_L$, $|+\rangle_L$ denote ancillary blocks encoded in the corresponding logical states in the *same* code as the data. The CNOT gates denote transversal CNOT gates acting between the data and ancillary blocks—the logical CNOT gate is transversal for CSS codes—and the measurements are understood as also being performed transversally. Evidently, as we would expect for error-correction circuitry, these circuits act trivially on the input logical information. However, their non-trivial content is that the outcomes of the transversal measurements reveal the *parity* of the code syndromes in the input and the ancillary

blocks.

We have seen that one way to specify $|0\rangle_L$ is via the stabilizer group in Eq. (5). In other words, our $|0\rangle_L$ is the state

$$|0\rangle_L = \bigotimes_{j=1}^n \left(\frac{|++\cdots+\rangle_{\text{col-j}} + |--\cdots-\rangle_{\text{col-j}}}{\sqrt{2}} \right) , (7)$$

where inside the parenthesis we have the state of the n qubits in column j in Fig. 1, and we have taken the tensor product of n identical such states on each one of the n columns. Similarly, our $|+\rangle_L$ is the state

$$|+\rangle_L = \bigotimes_{i=1}^n \left(\frac{|00\cdots 0\rangle_{\text{row-i}} + |11\cdots 1\rangle_{\text{row-i}}}{\sqrt{2}} \right) .$$
 (8)

Standard encoding circuits for the states in Eqs. (7) and (8) will be shown in Section E in this Appendix. We observe that the Hadamard-rotated cat states in Eq. (7) need only be verified [1] against multiple correlated Z errors but not against correlated X errors—any pair of X errors acts trivially on the state in Eq. (7). This implies that verification against correlated Z errors can be omitted if we repeat the syndrome measurement a certain number of times that depends on the distance of the code using different ancillary blocks. This is because only Xerrors can propagate from the $|0\rangle_L$ block to the data due to the direction of the CNOT gates, while here no correlated X errors can appear in $|0\rangle_L$. Similar observations hold for $|+\rangle_L$ for which verification against correlated X errors can also be avoided if we repeat the syndrome measurement.

Knill's FTEC method

Knill's FTEC method [12], shown schematically in Fig. 6, is more general than Steane's FTEC method as it applies to any stabilizer code. In this method, an ancillary logical Bell state is prepared and then transversal Bell measurements—i.e., measurements along the Bell basis $\{(Z^{j_1}X^{j_2}\otimes I)|\Phi_0\rangle\,|\,j_1,j_2=0,1\}$ —are performed between the input code block and one half of this ancilla. Finally, a logical Pauli operator is applied on the output code block in order to complete the logical teleportation of the input code state.

As in Steane's FTEC method, the outcomes of the transversal measurements reveal the parity of the code syndromes in the input block and the one half of the ancilla that is measured. First, this syndrome information allows us to perform error correction on the measurement outcomes. Then, we can compute parities on the, now corrected, measurement outcomes in order to obtain the eigenvalues of the logical $X \otimes X$ and $Z \otimes Z$ operators acting on the input code block and measured half of the ancilla. Because both the input block and the logical

Bell state are encoded in the same code, knowing the eigenvalues for these two logical operators allows us to complete the *logical* teleportation of the input code state by applying the appropriate logical Pauli correction $P(P_L)$ on the output code block. As usual, P_L need not actually be applied but can be kept in a classical memory as long as the succeeding logical operations are in the Clifford group [12].

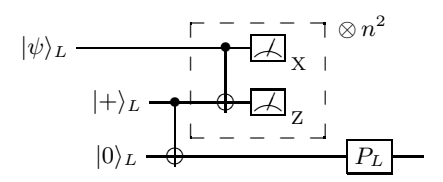


FIG. 6: A schematic of Knill's FTEC method for a code with n^2 qubits in the code block such as $\mathcal{C}_{BS}^{(n)}$. An ancillary logical Bell state is first prepared before transversal measurements along the Bell basis are performed between the input code block and one half of the ancilla. The measurement outcomes are constrained by parities which enable error correction. Then, the corrected measurement outcomes allow us to determine the logical Pauli operator P necessary to complete the logical teleportation of the input code state $|\psi\rangle_L$.

A remarkable feature of this FTEC method is that faults in the execution of the transversal Bell measurements can only result in an error in the logical Pauli operator P—if the logical Bell state is prepared without faults, the output code block is always in the code space independent of whether faults occurred in the transversal Bell measurements. The value of this observation comes when we consider performing an analysis of malignant sets of locations inside an extended rectangle [13] where Knill's FTEC method is used: Consider the leading FTEC gadgets inside the extended rectangle and let faults occur somewhere in the transversal Bell measurements. As we noted, these faults can only cause an error in P_L but cannot take the output code block outside the code space. Hence, these faults cannot combine with other faults elsewhere in the extended rectangle to form a malignant set. Therefore, for the purposes of this analvsis, the transversal Bell measurements in the leading FTEC gadgets in an extended rectangle can be taken as ideal! This reduces the number of locations that need to be considered in an analysis of malignant sets of locations and sheds light onto why Knill's FTEC method performs better than Steane's FTEC method for all codes analysed in Table I.

D. UNIVERSAL QUANTUM COMPUTATION

We have already discussed that the logical CNOT operation is transversal for the Bacon-Shor code: If we imagine bringing two square lattices as in Fig. 1 one on top of the other, applying CNOT gates bitwise will result in a

logical CNOT between the two protected qubits. In addition, the logical Hadamard is also transversal up to a 90-degree rotation of the lattice. By combining the logical CNOT with the logical Hadamard, we find that the logical controlled-Z or CPHASE gate is also transversal since it can be implemented by doing a logical Hadamard on the target, followed by a logical CNOT, followed by another logical Hadamard on the target.

A destructive measurement of the logical X (resp. Z) operator can be performed by transversally measuring the operator X (resp. Z) on each qubit in the code block. (With the logical CNOT and CPHASE transversal, we can also measure non-destructively the logical X or the logical Z operator by using as control an ancilla prepared in the logical $|+\rangle$ state.) If we were also able to easily measure the logical Y = iXZ operator (Y_L) , we would be able, e.g., by using the circuit in Fig. 7, to implement the logical phase gate $S \equiv \exp(-i\frac{\pi}{4}\sigma_z)$. The logical CNOT, Hadamard and phase gates would then be sufficient for generating the logical Clifford group.

$$|\psi\rangle \longrightarrow Y$$

$$|0\rangle \longrightarrow Z - S|\psi\rangle$$

FIG. 7: Circuit simulation of the phase gate S using a measurement of Y.

Although $Y_L = \bigotimes_{i=1}^{n^2} Y^{(i)}$ when n is odd, measuring transversally the operators $Y^{(i)}$ does not give a fault-tolerant measurement of Y_L . This is because the Bacon-Shor code has no stabilizer operators which can be written as tensor products of Y operators alone. Therefore, the problem is that we cannot perform error correction on the transversal measurement outcomes and, so, the eigenvalue we would deduce for the logical Y could be erroneous even if a single one of the transversal measurements failed.

We could instead measure the logical Y operator nondestructively using cat states [1, A2]. Implementing this measurement would require controlled-Y gates which, at the next level of concatenation, would have to be implemented in an encoded form. But then, the problem is that the controlled-Y gate is complex and all the transversal operations we have discussed so far (CNOT, CPHASE and Hadamard) are real. Hence, we don't have a direct fault-tolerant method for implementing the logical controlled-Y gate.

Fortunately, as we will discuss next, there is a method for simulating the logical S gate by using only logical CNOT and CPHASE gates provided we can fault-tolerantly prepare a certain logical ancillary state. To complete quantum universality, we also need to simulate some logical gate outside the Clifford group; we will take this to be the Toffoli gate (controlled-controlled-X or $\Lambda^2(X)$) or some real non-Clifford single-qubit rotation.

We will next describe how the logical S and Toffoli gates can be simulated fault-tolerantly, i.e., in a way that satisfies properties 2 and 3 in $\S 9$ in [13]. Our discussion is borrowed from the universality construction for the Bravyi-Kitaev surface code in [A3]. The fact that universality can be achieved in the same way for these two codes is not surprising; as we discussed in Section A of this Appendix, the Bacon-Shor code can be viewed as a reduction of the Bravyi-Kitaev surface code after some qubits outside of the support of the logical Pauli operations of the code have been measured.

The logical S gate

Consider the states $|\pm i\rangle \propto |0\rangle \pm i|1\rangle$ which are the ± 1 eigenstates of Y. Given the state $|+i\rangle$, we can simulate S (up to an irrelevant phase) on some input state $|\psi\rangle$ using the circuit in Fig. 8. Furthermore, if the state $|-i\rangle$ is used instead in the same circuit, then the operation $S^{\dagger} = S^*$ will be simulated. Since the logical CNOT and CPHASE can be implemented transversally, the problem of simulating the logical S gate fault-tolerantly reduces to the problem of fault-tolerantly preparing the logical ancillary state $|+i\rangle$ or $|-i\rangle$.

$$|\psi\rangle$$
 $e^{i\pi/4}S|\psi\rangle$ $|+i\rangle$ Z $|+i\rangle$

FIG. 8: Circuit simulation of the phase gate S using the ancillary state $|{+}i\rangle.$

Simulating S and S^* in superposition

Based on the circuit in Fig. 8, we will now first describe a surprisingly simple procedure by which the simulation of the logical S gate is still possible even if the logical ancillary state $|+i\rangle$ is replaced by another logical ancillary state which is easier to prepare [A3]. This procedure makes use the fact that the S gate is the only complex gate in our universal gate set.

Consider using some standard state, say the state $|0\rangle$, instead of $|+i\rangle$ in the circuit in Fig. 8. We can expand $|0\rangle \propto |+i\rangle + |-i\rangle$ and, for each of the two terms, we can consider the two paths of the subsequent computation which are executed in superposition. In one path S is simulated and in the other S^* . Thus, if every time we want to simulate S in our circuit we use the same ancillary $|0\rangle$ state and because S is the only complex gate in our gate set, the final state of the computation will be a linear superposition of one term where the desired computation unitary U has been implemented and a second term where U^* has been implemented instead. In other

words, if the initial computation state is $|\psi_{\text{initial}}\rangle$, then the final computation state will be

$$|\psi_{\text{final}}\rangle \propto |+i\rangle \otimes U|\psi_{\text{initial}}\rangle + |-i\rangle \otimes U^*|\psi_{\text{initial}}\rangle$$
. (9)

In the end of the computation some operator A will be measured which we can take to be real (and so, due to hermiticity, $A^T = A$). We now want to see that the expectation value for A will be the same as if the desired U had been simulated all along. Indeed, we compute

$$\langle A \rangle = \langle \psi_{\text{initial}} | \frac{U^{\dagger} A U + (U^*)^{\dagger} A U^*}{U^{\dagger} A U} | \psi_{\text{initial}} \rangle$$

$$= \langle \psi_{\text{initial}} | U^{\dagger} A U | \psi_{\text{initial}} \rangle , \qquad (10)$$

since,
$$\forall |\psi\rangle$$
, $\langle \psi|(U^*)^{\dagger}AU^*|\psi\rangle = \langle \psi|U^{\dagger}A^TU|\psi\rangle = \langle \psi|U^{\dagger}AU|\psi\rangle$.

We can use this procedure at the logical level as well. The only penalty we pay for simulating the logical S gate in this way is that we need to swap around the ancillary $|0\rangle_L$ block we use for the simulation if we are constrained to use only geometrically local interactions—but, this will only give us a linear penalty in the size of the computation. Of course, we should emphasize that this trick works because the S gate is not used in implementing error correction and, as a consequence, it is not necessary that we execute different S gates in parallel anywhere in our computation. In addition, since the simulation uses only CNOT and CPHASE gates and the preparation of the $|0\rangle$ state, the logical S gate does not need to be considered separately in our analysis for determining the accuracy threshold.

Noisy $|+i\rangle$ purification

If we had not read [A3] to know about the previous trick, we could also use more straightforward methods to fault-tolerantly prepare the state $|+i\rangle_L$. For instance, we could begin by preparing many noisy $|+i\rangle_L$ states—e.g., by using teleportation to "inject" the single-qubit state $|+i\rangle$ into a code block [12]—and we could subsequently purify them; a possible purification circuit is shown in Fig. 9.

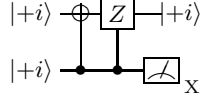


FIG. 9: Circuit for the non-deterministic purification of the state $|+i\rangle$. Post-selecting on the measurement outcome being -1, the output $|+i\rangle$ state has quadratically improved fidelity.

The measurement outcome in the circuit above is ideally -1, and an error on *one* of the two input states can be detected. We note that, because Y stabilizes the state $|+i\rangle$, we need only worry about Z errors—we can write X = iZY which is, up to the irrelevant phase i,

equivalent to Z when it acts on $|+i\rangle$. Post-selecting on getting the measurement outcome -1, the fidelity of the noisy output state is increased quadratically relative to the fidelity of the input states—it takes errors in both input $|+i\rangle$ states for an error in the output state to go undetected.

The purification procedure can also be implemented deterministically using the circuit in Fig. 10, this time using three input $|+i\rangle$ states. Ideally both measurements outcomes in this circuit give outcome -1. If both outcomes are +1 then, to first order in the error parameter, a Z error has occurred on the first $|+i\rangle$ state and, hence, a Z correction must be applied on the output state to invert it. The fidelity of the noisy output state is again improved quadratically relative to the fidelity of the input states after one execution of the protocol.

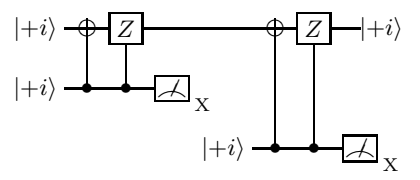


FIG. 10: The deterministic counterpart of the purification circuit in Fig. 9. A Z correction is applied on the output $|+i\rangle$ state if both measurement outcomes are +1, else no correction is applied. Again, the fidelity of the output is improved quadratically after one run of the protocol.

The logical Toffoli gate

The simulation of the logical Toffoli gate uses the logical ancillary state $|\text{Toffoli}\rangle \equiv \Lambda^2(X) \, (|+\rangle \otimes |+\rangle \otimes |0\rangle)$ in the circuit in Fig. 11 [1, A4]. Depending on the measurement outcomes $j_{\{1,2,3\}} = \pm 1$, the post-measurement Clifford-group corrections are $X^{(1)} \otimes \text{CNOT}_{2 \to 3}$ if $k_1 = 1$, $X^{(2)} \otimes \text{CNOT}_{1 \to 3}$ if $k_2 = 1$, and $\text{CPHASE}_{1,2} \otimes Z^{(3)}$ if $k_3 = 1$, where $k_{\{1,2,3\}} = (1-j_{\{1,2,3\}})/2$.

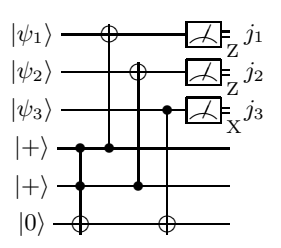


FIG. 11: Circuit simulation of the Toffoli gate using the ancilla |Toffoli⟩. The post-measurement Clifford-group corrections that depend on the measurement outcomes are not shown.

Therefore, as in the simulation of the logical S gate, the problem of simulating the logical Toffoli gate fault-tolerantly reduces to fault-tolerantly preparing a logical ancillary state, the logical $|\text{Toffoli}\rangle$.

Noisy |Toffoli\rangle preparation by concatenation

 $|\text{Toffoli}\rangle$ is the +1 eigenstate of the three operators $S_1 = X^{(1)} \otimes \text{CNOT}_{2 \to 3}$, $S_2 = X^{(2)} \otimes \text{CNOT}_{1 \to 3}$ and $S_3 = \text{CPHASE}_{1,2} \otimes Z^{(3)}$. Then, consider starting with the state $|+\rangle^{\otimes 3}$ which is clearly a +1 eigenstate of both S_1 and S_2 . To obtain the state $|\text{Toffoli}\rangle$ it now remains to perform a measurement of the operator S_3 . This can be accomplished with the circuit in Fig. 12 [1, A4].

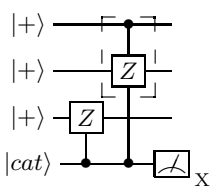


FIG. 12: A circuit that projects the input state $|+\rangle^{\otimes 3}$ onto the +1 eigenstate of the operator S_3 depending on the measurement outcome. For outcome +1 the output state is |Toffoli⟩.

If this circuit were executed in an un-encoded form, then the cat state would simply be one qubit in the state $|+\rangle$. However, the logical circuit will be executed instead and, then, the cat state is $|\bar{+}\rangle \propto |\bar{0}\rangle + |\bar{1}\rangle$, i.e., the logical $|+\rangle$ state in the n^2 -bit classical repetition code $C_Z^{(n^2)}$. The cat state must either be verified against X errors, or a decoding circuit can replace the transversal measurements in order to avoid verification [A5].

Since the circuit in Fig. 12 is realized in an encoded form, the first three states are logical $|+\rangle$ states and logical CPHASE and controlled-controlled-Z gates need be performed. Then, we observe that the logical controlled-controlled-Z or $\Lambda^2(Z)$ gate can be implemented using transversal $\Lambda^2(Z)$ gates since the CPHASE is transversal; the qubits in one of the first two code blocks need to be rotated by 90 degrees before bitwise $\Lambda^2(Z)$ gates are applied and then the qubits need to be rotated back by 90 degrees. Conjugating with bitwise Hadamard gates on the cat-state qubits, the bitwise $\Lambda^2(Z)$ gates become bitwise Toffoli gates which allows this same circuit to be executed in a higher coding level as well.

The above procedure requires concatenation in order to increase the fidelity of the ancillary state |Toffoli⟩. To improve the accuracy threshold below which concatenation will reduce the logical error rate of this state, we can bootstrap the |Toffoli⟩ preparation in Fig. 12 to start at a higher coding level than the first coding level. That is, we can implement the Toffoli gates in the circuit in Fig. 12 at a sufficiently high level of concatenation using the simulation circuit in Fig. 11 and |Toffoli⟩ ancillae prepared, e.g., by state-injection [12]. Although these logical ancillae will have an error rate of the order of the physical error rate, the logical error rates of all Clifford-group operations in the circuits in Figs. 11 and 12 can be made arbitrarily small provided we operate below the threshold of Clifford-group computation. Because of this, the accu-

racy threshold for the |Toffoli⟩ preparation will be significantly higher than the threshold for Clifford-group gates which, therefore, will set the overall accuracy threshold.

Noisy |Toffoli\) purification

As an alternative to concatenation, we could consider preparing several copies of the logical |Toffoli \rangle state—again, e.g., by using state-injection [12]—and purifying them [A6, A7]. Let us then construct a circuit that takes as an input some number of copies of the |Toffoli \rangle state and outputs one |Toffoli \rangle state of improved fidelity.

Consider the circuit in Fig. 13. We start with one copy of the state $|\text{Toffoli}\rangle$ and measure the operator S_1 using one ancillary qubit initialized in the state $|+\rangle$. Since the state $|\text{Toffoli}\rangle$ is an eigenstate of this operator, the effect of the measurement is trivial: the first three qubits remain in the state $|\text{Toffoli}\rangle$ and the measurement on the ancilla always ideally gives outcome +1.

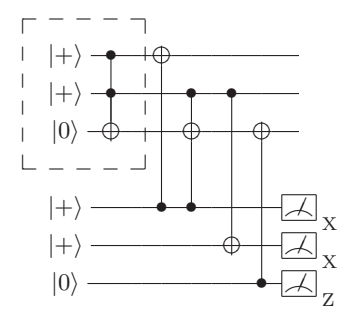


FIG. 13: A circuit that uses one ancillary qubit to measure the operator $S_1 = X^{(2)} \otimes \text{CNOT}_{1 \to 3}$ on the input |Toffoli \rangle state. The measurement outcome is ideally +1 since |Toffoli \rangle is an eigenstate of S_1 . Note that the gates acting on the second and third ancillae operate trivially.

The circuit in Fig. 13 includes two extra ancillae. These qubits are useful because we now want to insert two cancelling Toffoli gates acting on the ancillae in this circuit. We thus obtain the equivalent circuit shown in Fig. 14. Our motivation for inserting the resolution of the identity in the form of the two Toffoli gates is to create two copies of the state |Toffoli⟩ in the input of the circuit. Thus, we next commute the left-most of the two Toffoli gates to the left of the circuit using repeatedly the circuit identities in Fig. 15. After the dust settles, the result is the circuit shown in Fig. 16.

Except for the two input |Toffoli⟩ states, this circuit includes additional Toffoli gates acting between these two states which we do not know how to perform fault-tolerantly—recall that our goal is to design a purification circuit for the |Toffoli⟩ state that uses exclusively Clifford-group operations. However, if we measure the last two qubits in this circuit as shown in Fig. 17, we can apply corrections depending on the measurement outcomes that will restore the state of the first three qubits

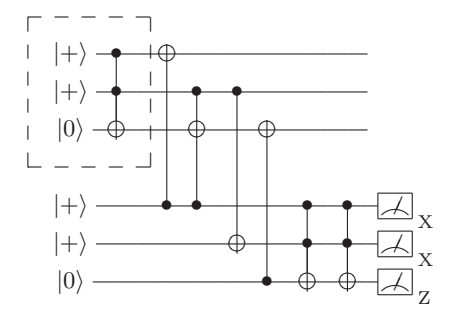


FIG. 14: The circuit in Fig. 13 where a pair of cancelling Toffoli gates have been inserted.

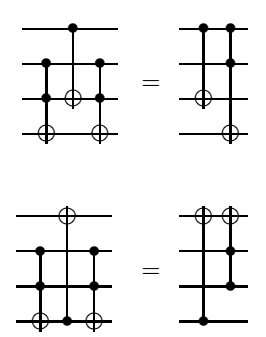


FIG. 15: Commutation relations of CNOT and Toffoli.

to be the state |Toffoli).

Furthermore, if we subsequently measure the fourth qubit, we will obtain the product of the eigenvalues of S_1 acting on the two input copies of the state |Toffoli \rangle . Ideally, this product is +1 because both of these states are eigenstates of S_1 . Hence, if the measured product is -1, we know that one of the input copies had an error. In that case we can either reject both copies and start over or, to make the purification procedure deterministic, we can use a third copy of the state |Toffoli> and compare the surviving copy from this round of purification with this new state. If a -1 product is measured again, then we know that, to first order in the error parameter, the error has occurred in the first copy and we can proceed to correct it. Otherwise, we become more confident that the first copy is an eigenstate of S_1 as desired. Overall, by using either the deterministic or the non-deterministic purification procedure, the fidelity of the noisy output state improves.

In more detail, the 2^3 eigenstates of the three commuting operators S_1 , S_2 and S_3 form an orthonormal basis in the three-qubit Hilbert space. Moreover, the state $|\text{Toffoli}\rangle$ that we want to purify is the +1 eigenstate of these operators; therefore, it is one of the basis states in this basis. We can label any state in this basis by three numbers $a,b,c=\pm 1$ corresponding to its eigenvalues with respect to the operators S_1 , S_2 and S_3 , and let a basis state with parameters a,b,c be denoted $|\text{Toffoli}\rangle_{a,b,c}$. Then, if the input to the purification circuit in Fig. 17 is the two states $|\text{Toffoli}\rangle_{a,b,c}$ and

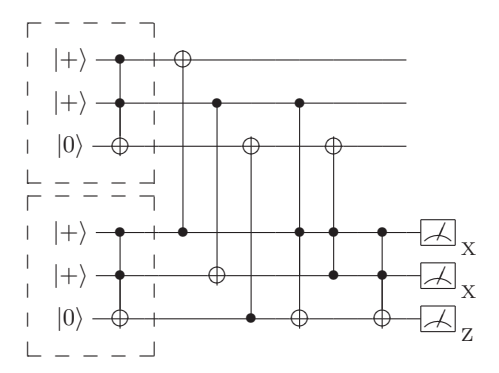


FIG. 16: An equivalent circuit to that in Fig. 13. We identify the input to be two copies of the state |Toffoli⟩ shown in boxes.

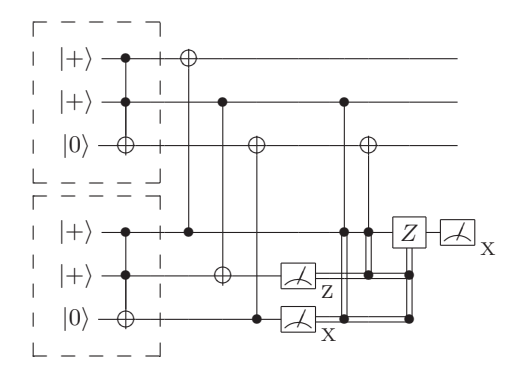


FIG. 17: After measuring the last two qubits in Fig. 16 and applying the appropriate corrections, the first three qubits are left in the state |Toffoli \rangle . The fourth qubit is then measured with the outcome giving the product of the eigenvalues of S_1 acting in the two input |Toffoli \rangle states.

 $|\text{Toffoli}\rangle_{a',b',c'}$, the first three qubits at the output are in the state $|\text{Toffoli}\rangle_{a,b\cdot b',c\cdot c'}$. Moreover, the measurement outcome on the fourth qubit corresponds to $a\cdot a'$, i.e., it equals the product of the eigenvalues of S_1 of the two input copies.

Thus, the circuit in Fig. 17 improves the fidelity of the surviving state $|\text{Toffoli}\rangle_{a,b\cdot b',c\cdot c'}$ with respect to the parameter a, but the parameters b and c get worse—if any one of the input copies was a -1 eigenstate of S_2 or S_3 , then the surviving copy will also be such a -1 eigenstate. However, the fidelity with respect to the parameters b and c only gets worse by a linear factor whereas the fidelity with respect to a improves quadratically [A6, A7]. Therefore, if we repeat the purification protocol using another circuit that purifies with respect to the b parameter and also with a third circuit that purifies with respect to c, we will achieve a quadratic improvement in the fidelity with respect to all three parameters a, b and c. Such circuits can be constructed using a similar trick as the one we used to derive the circuit in Fig. 17 from that in Fig. 13.

Alternative paths to universality

The logical T_v gate

Instead of the Toffoli, we could use the real non-Clifford gate $T_{\rm y} \equiv \exp(-i\frac{\pi}{8}\sigma_{\rm y})$ to obtain a quantum universal gate set. To simulate $T_{\rm y}$ it is sufficient to prepare the +1 eigenstate of the Hadamard gate, $|H\rangle \equiv \cos(\frac{\pi}{8})|0\rangle + \sin(\frac{\pi}{8})|1\rangle$, and use the circuit in Fig. 18.

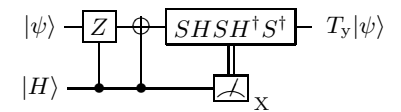


FIG. 18: Circuit simulation of the gate T_y using the ancillary state $|H\rangle$.

The purification of the ancilla $|H\rangle$ can be done non-deterministically as discussed in Refs. [A8] and [A9]. Assuming Clifford-group gates are ideal, the threshold accuracy for $|H\rangle$ distillation is at least $1-0.927^2 \geq 14\%$ [A9], which is significantly higher than the accuracy threshold for Clifford-group operations.

Bootstrapping another code with transversal logical S gate

Alternatively, we could use the Bacon-Shor code for the initial levels of concatenation only and then bootstrap another code with more convenient universality properties. For example, the Bacon-Shor code could be concatenated sufficiently many times until the logical error rate for the CNOT and Hadamard gates and for the measurement of logical Pauli operators at the highest level becomes significantly lower than the threshold for the [[7,1,3]] code for which the logical S gate is transversal. At the first level where the new bootstrapped code is to be used, logical ancillary states that enable the simulation of the logical S and the non-Clifford $T \equiv S^{1/2}$ gates at the highest level of the concatenated Bacon-Shor code could be constructed using, e.g., state-injection [12].

E. ACCURACY THRESHOLD LOWER BOUNDS

The [[4,1,2]]
$$C_{BS}^{(2)}$$
 code

 $C_{BS}^{(2)}$ is a one-error detecting code with one gauge qubit. Its stabilizer group and the logical Pauli operators for the protected and the gauge qubit are, respectively,

$$S(C_{BS}^{(2)}) = \langle X_{\text{row}-1,\text{row}-2}; Z_{\text{col}-1,\text{col}-2} \rangle ;$$

$$L = \{ X_{\text{row}-1}; Z_{\text{col}-1} \} ;$$

$$T = \{ X_{\text{col}-1}; Z_{\text{row}-1} \} .$$
(11)

For this code, Steane's FTEC method and our new FTEC method that uses measurements on the gauge qubits are identical in the following sense: Consider our logical $|0\rangle$ state. It consists of two Hadamard-rotated cat states aligned along the two columns. But, a twoqubit cat state is the same as a Bell state and Bell states are the same in the computation and in the Hadamardrotated basis. Thus, a measurement of the syndrome using a $|0\rangle_L$ ancilla is the same as running the circuit in Fig. 4(b) in parallel in the two columns for the measurement of $X_{1,1}X_{2,1}$ and $X_{1,2}X_{2,2}$. Clearly, by combining the outcomes of these two measurements, we can deduce the eigenvalue of the stabilizer generator $X_{\text{row}-1,\text{row}-2}$. Doing a similar measurement across the two rows will give us the eigenvalue of the other stabilizer generator $Z_{\text{col}-1,\text{col}-2}$.

Because $C_{BS}^{(2)}$ only enables error detection, techniques based on postselection similar to those discussed in Refs. [12, A8] are necessary to obtain an accuracy threshold by concatenation. We have not analysed such a scheme in this paper.

The [[9,1,3]]
$$C_{BS}^{(3)}$$
 code

 $\mathcal{C}_{BS}^{(3)}$ is a one-error correcting code with four gauge qubits. Its stabilizer group is

$$S(C_{BS}^{(3)}) = \langle X_{\text{row}-1,\text{row}-2}; X_{\text{row}-2,\text{row}-3}; \\ Z_{\text{col}-1,\text{col}-2}; Z_{\text{col}-2,\text{col}-3} \rangle,$$
 (12)

and the logical Pauli operations for the protected qubit are, again, $\bar{X} = X_{\text{row}-1}$ and $\bar{Z} = Z_{\text{col}-1}$. The logical Pauli operators for the four gauge qubits are operators chosen appropriately from this group T that consists of operators with an even number of Z operators in each row and an even number of X operators in each column.

Circuits for FTEC using measurements on the gauge qubits are shown in Fig. 19. Because, e.g., a Z error on both qubits acted upon by the second CNOT operating on qubit (2,j) will flip the eigenvalue of the measured operator $X_{1,j}X_{2,j}$ and also create a $Z_{2,j}$ error in the data, the measurement of an extra operator is necessary for fault tolerance [A10]; in Fig. 19 we have chosen to measure the extra operator $X_{1,j}X_{3,j}$. This extra measurement provides the necessary redundancy in order to avoid having one fault cause a logical error in the data block.

Alternatively, in order to obtain the syndrome for Z errors with Steane's FTEC method, we need to prepare the ancillary state $|0\rangle_L$ which consists of three Hadamard-rotated cat states aligned across the three columns; for column j the circuit is, therefore, as in Fig. 20(a). To obtain the syndrome for X errors, we prepare a logical $|+\rangle$ state which consists of cat states along the three rows; for row i the circuit is shown in Fig. 20(b). We observe that

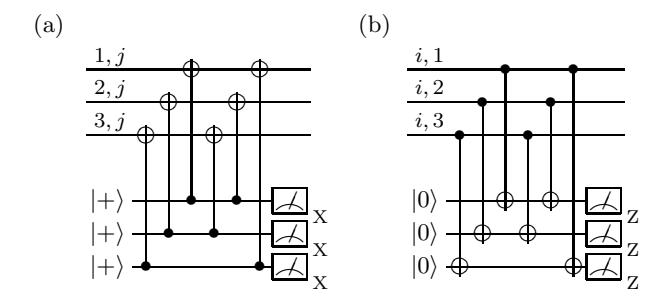


FIG. 19: FTEC for $C_{BS}^{(3)}$ using measurements on the gauge qubits. (a) Measuring operators in T along column j. (b) Measuring operators in T along row i. Identical circuits are run in parallel for all rows and columns. In both circuits, the third measurement is used to provide an extra redundancy bit. For maximum qubit-efficiency, all measurements could be implemented sequentially using the same one ancillary qubit.

these circuits have the remarkable property that they are fault tolerant without the need to verify the different cat states. Indeed, consider a faulty CNOT inside the encoding circuit for these cat states. A X error on both qubits acted upon by this gate is either i) an operator in the cat-state stabilizer in Fig. 20(a) or, ii) is equivalent to a single X error on the other qubit in Fig. 20(b). Similarly for a Z error acting on both qubits. Otherwise, a X error acting on one qubit and a Z error on the other cannot lead to more than one X and/or one Z error propagating from the cat state to the data block. Thus, properties 0 and 1 in [13] are satisfied [A11].

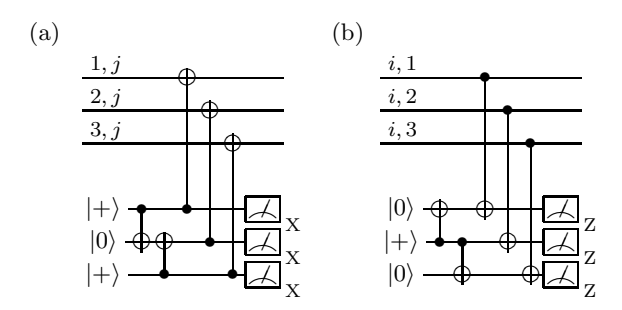


FIG. 20: Steane's FTEC method for $C_{BS}^{(3)}$. (a) Collecting the syndrome for Z errors. The circuit in column j is shown. (b) Collecting the syndrome for X errors. Here, the circuit for row i is shown. Identical circuits are run in parallel for all three rows and columns.

The circuitry for Knill's FTEC method also uses threequbit cat states and transversal CNOT gates for preparing a logical Bell state. As with the encoded ancillae for Steane's FTEC method, this preparation circuit for the logical Bell state is also fault tolerant without the need for ancilla verification. Moreover, the circuits for Steane's and Knill's FTEC methods contain exactly the same number of locations.

A crude lower bound on the accuracy threshold can be obtained by counting the total number of pairs of locations inside the CNOT extended rectangle [13]. The FTEC circuit for Steane's method contains 72 qubit-preparation, measurement, gate or memory locations. The CNOT extended rectangle therefore contains $4\times72+9=297$ locations and, so, we obtain a threshold lower bound of $\binom{297}{2}^{-1} \geq 2.2\times10^{-5}$. Let us denote by ε_i the upper bound on the error prob-

Let us denote by ε_i the upper bound on the error probability associated with location type i, where locations are labeled as (1) memory, (2) $|0\rangle$ preparation, (3) $|+\rangle$ preparation, (4) measurement of X, (5) measurement of Z and (6) CNOT. A detailed analysis of malignant pairs of locations [13] using Steane's FTEC method gives for the error probability of the level-k CNOT extended rectangle:

$$\varepsilon_6^{(k)} \le \sum_{j \le i=1}^6 \alpha_{ij} \,\varepsilon_i^{(k-1)} \varepsilon_j^{(k-1)} + B_6 \left(\varepsilon_{\max}^{(k-1)}\right)^3, \quad (13)$$

where $\varepsilon_{\max}^{(k-1)} = \max_i \{ \varepsilon_i^{(k-1)} \}$ (with our choice of a quantum universal gate set, $\varepsilon_{\max}^{(k-1)} = \varepsilon_6^{(k-1)}$). Third or higher order events contribute $B_6 \equiv \binom{297}{3} \leq 4.33 \times 10^6$ and the coefficients α_{ij} were found by a computer-assisted combinatorial analysis to be

$$\alpha = \begin{pmatrix} 52 \\ 174 & 138 \\ 174 & 0 & 138 \\ 234 & 0 & 378 & 216 \\ 234 & 378 & 0 & 0 & 216 \\ 1154 & 1281 & 1281 & 1566 & 1556 & 3733 \end{pmatrix}.$$
 (14)

Taking the error probabilities $\{\varepsilon_i\}$ for all locations to be equal to $\max_i \{\varepsilon_i\}$, we obtain $A_6 = 12,913$ malignant pairs, or

$$\varepsilon_6^{(k)} \le A_6' \left(\varepsilon_6^{(k-1)} \right)^2 , \tag{15}$$

where $A_6' = \frac{A_6}{2} \left(1 + \sqrt{1 + \frac{4B_6}{A_6^2}} \right) = 13,241$. This indicates 7.55×10^{-5} as a lower bound on the accuracy threshold.

We can improve this bound moderately if we use the idea of contracted extended rectangles (called stretched in [A12]), i.e., if we omit FTEC steps at levels $k \geq 2$ wherever they are not necessary. In particular, we can contract state-preparation extended rectangles and join them with the succeeding CNOT extended rectangles and, similarly, contract measurement extended rectangles to join them with the preceding CNOT extended rectangles. Then, for all levels $k \geq 2$, we need not consider separate preparation or measurement extended rectangles at level k-1. Instead, we can consider level-(k-1) contracted extended rectangles that contain level-(k-1) preparation (resp. measurement) joined with the succeeding (resp. preceding) level-(k-1) CNOT operations and the intermediate level-(k-1) FTEC omitted. We observe that such contracted extended rectangles have error rates no worse than the standard CNOT extended rectangles because i) FTEC following state preparation is superfluous

as long as the encoding circuit is made fault tolerant using, e.g., state verification, and ii) measurement is performed transversally and so classical error correction on the measurement outcomes can replace quantum error correction preceding the measurements.

Thus, for levels $k \geq 2$, we can effectively set those coefficients in Eq. (14) that involve preparation or measurement locations to zero. Then, for levels $k \geq 2$, we compute $A_{6,\rm str} = 4,939$, $B_{6,\rm str} = \binom{153}{3} \leq 5.86 \times 10^5$ and so $A'_{6,\rm str} \leq 5,055$. Thus, we obtain the recursion equations

$$\varepsilon_{6}^{(1)} \leq 13,241 (\varepsilon_{6})^{2},
\varepsilon_{6}^{(k)} \leq 5,055 (\varepsilon_{6}^{(k-1)})^{2} \text{ for } k > 1,$$
(16)

which imply the condition $\varepsilon_6^{(1)} < 1.97 \times 10^{-4}$ or $\varepsilon_6 < 1.21 \times 10^{-4}$. Hence, 1.21×10^{-4} is our accuracy threshold lower bound for adversarial stochastic noise.

If we use Knill's FTEC method instead, the analogous coefficients α_{ij} of Eq. (13) are found to be

$$\alpha = \begin{pmatrix} 60 \\ 60 & 30 \\ 60 & 0 & 30 \\ 180 & 0 & 180 & 270 \\ 180 & 180 & 0 & 0 & 270 \\ 1104 & 552 & 552 & 1656 & 1656 & 4164 \end{pmatrix} . \tag{17}$$

Repeating the calculation above, we find $A_6=11,184$ and $A_6'\leq 11,558$. This indicates a lower bound of 8.65×10^{-5} on the accuracy threshold. This bound can also be improved if we use contracted extended rectangles. For levels $k\geq 2$, we compute $A_{6,\rm str}=5328$. Furthermore, because of our observation in Section C in this Appendix, we can take the transversal Bell measurements in the leading FTEC circuits inside the CNOT extended rectangle to be ideal. This reduces the effective number of locations in this extended rectangle from $297 \times 297 = 243$ at level 1, and from $153 \times 297 = 243$ at level 1, and from $153 \times 297 = 243$ at level 1, and from $153 \times 297 = 2135$ at levels 126×10^{-4} as our accuracy threshold lower bound using Knill's FTEC method.

The [[25,1,5]]
$$C_{BS}^{(5)}$$
 code

 $\mathcal{C}_{BS}^{(5)}$ is a two-error correcting code with sixteen gauge qubits. Despite its large block size relative to its distance, our fault-tolerant quantum circuits are more efficient than for other interesting CSS codes of high distance as, e.g., the Golay [[23,1,7]] code. In fact, Table I shows that the CNOT extended rectangle for $\mathcal{C}_{BS}^{(5)}$ contains 1,185 locations, when the corresponding extended rectangle for the Golay code contains 7,551 locations [Reichardt, Ouyang; unpublished].

FTEC using measurements on the gauge qubits can be implemented with the circuits shown in Fig. 21. In order to satisfy properties 0 and 1 in [13], we need to add some redundancy in our syndrome measurements; e.g., syndrome extraction could be repeated.

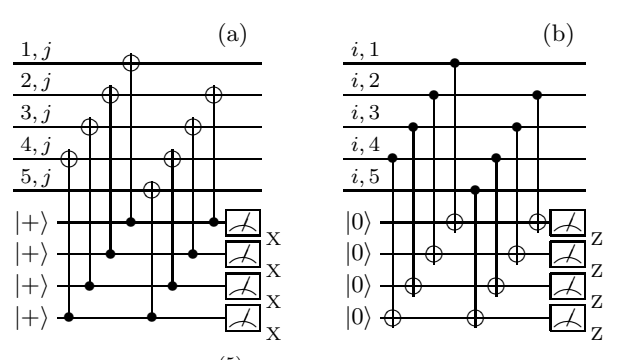


FIG. 21: FTEC for $C_{BS}^{(5)}$ using measurements on the gauge qubits. (a) Measuring operators in T along column j. (b) Measuring operators in T along row i. Identical circuits are run in parallel for all rows and columns $i, j \in \mathbb{Z}_5$. Some form of redundancy is necessary to ensure fault tolerance; e.g., the syndrome extraction could be repeated. Again, all these measurements could be executed sequentially using a single ancillary qubit.

For Steane's FTEC method, we prepare five-qubit cat states, e.g., as shown in Fig. 22. This time the cat states need verification to prevent a single fault from causing more than one X and/or Z error that will propagate to the subsequent transversal measurements. Alternatively, verification can be replaced by repeated syndrome extraction. These cats states can be used to collect the syndrome similarly to Fig. 20 for $C_{BS}^{(3)}$.

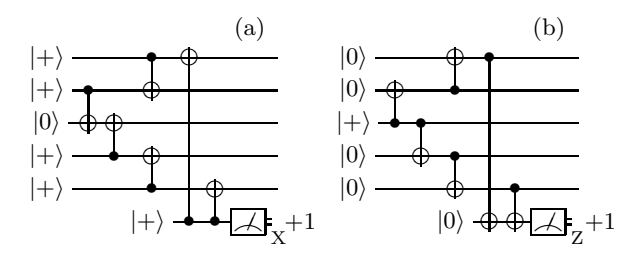


FIG. 22: (a) A five-qubit cat state in the Hadamard-rotated basis with verification against Z errors. (b) A five-qubit cat state with verification against X errors.

An analysis of malignant triples of locations gives for the *joint* probability of error for the level-k CNOT extended rectangle and a successful outcome in all of the verification tests:

$$\varepsilon_{6,\text{joint}}^{(k)} \le \sum_{\ell \le j \le i=1}^{6} \alpha_{ij\ell} \varepsilon_i^{(k-1)} \varepsilon_j^{(k-1)} \varepsilon_\ell^{(k-1)} + B_6 (\varepsilon_{\text{max}}^{(k-1)})^4 ,$$
(18)

where $B_6 = \binom{1185}{4}$ gives the number of combinations of four locations inside the CNOT 1-exRec which contains

1,185 locations in total. As in [13], the probability of a successful outcome in a verification test is

$$P_{\text{accept}}^{(k)} \ge \left(1 - \varepsilon_{\text{max}}^{(k-1)}\right)^{C_6},\tag{19}$$

where C_6 is the total number of locations in the encoding and verification circuit for all cat states contained in one FTEC circuit. Taking the error probabilities $\{\varepsilon_i\}$ for all locations to be equal to $\max_i \{\varepsilon_i\}$, the error probability of the level-k CNOT extended rectangle *conditioned on* the successful outcome in all verification tests is

$$\varepsilon^{(k)} \le \left(1 - \varepsilon^{(k-1)}\right)^{-4C_6} (A_6 + B_6 \varepsilon^{(k-1)}) (\varepsilon^{(k-1)})^3, (20)$$

where $A_6 = 16,625,488$ is the total number of malignant triples and $C_6 = 190$.

As we did for $C_{BS}^{(3)}$, for all concatenation levels $k \geq 2$, we can consider contracted extended rectangles. Then, for levels $k \geq 2$ we only keep the coefficients $\alpha_{ij\ell}$ that do not involve preparation or measurement locations. Since $\alpha_{111} = 287,460$, $\alpha_{116} = 1,899,918$, $\alpha_{166} = 3,911,460$, and $\alpha_{666} = 2,554,190$, we have $A_{6,\text{str}} = 8,653,028$. From the FTEC circuits, we have $B_{6,\text{str}} = \binom{705}{4}$ and $C_{6,\text{str}} = 120$. Solving for the fixed point of our recursion equations, we obtain 1.94×10^{-4} as our lower bound on the accuracy threshold.

The circuit constructions and threshold analysis for $C_{BS}^{(7)}$ are similar to $C_{BS}^{(3)}$ and $C_{BS}^{(5)}$ and will be omitted.

[A1] S. Bravyi and A. Yu. Kitaev. arXive e-print quant-ph/9811052.

- [A2] D. P. DiVincenzo and P. Shor. Phys. Rev. Lett. 77, 3260 (1996). arXive e-print quant-ph/9605031.
- [A3] E. Dennis, A. Kitaev, A. Landahl, and J. Preskill. J. Math. Phys. 43, 4452 (2002). arXive e-print quant-ph/0110143.
- [A4] J. Preskill. Introduction to Quantum Computation, p. 213–269, eds. H.-K. Lo and S. Popescu and T. P. Spiller, World Scientific, Singapore (1998). arXive e-print quant-ph/9712048.
- [A5] D. P. DiVincenzo and P. Aliferis. Phys. Rev. Lett. 98, 020501 (2007). arXive e-print quant-ph/0607047.
- [A6] D. Gottesman. Problem 4, set 5, C&O 639, University of Waterloo, 2004. http://www.perimeterinstitute.com/personal/dgottesman/CO639-2004/
- [A7] J. Preskill. Ph/CS 219, Caltech, 2005. http://www.theory.caltech.edu/people/preskill/ph229/
- [A8] E. Knill. arXive e-print quant-ph/0402171.
- [A9] S. Bravyi and A. Yu. Kitaev. Phys. Rev. A 71, 022316 (2005). arXive e-print quant-ph/0403025.
- [A10] An error in the eigenvalue of $X_{1,j}X_{2,j}$ will lead us to incorrectly infer an error $Z_{1,j}$ in the data if we do not perform the extra measurement of $X_{1,j}X_{3,j}$. Combining $Z_{1,j}$ with $Z_{2,j}$ leads to an uncorrectable error in the data caused by a single faulty CNOT.
- [A11] One X and one Z error in different data qubits is not, strictly speaking, acceptable since the resulting state has a weight-two error and will not pass through a 1-filter [13]. However, for the CNOT, CPHASE and Hadamard extended rectangles which determine the accuracy threshold (the logical phase and Toffoli gates can be implemented at the highest concatenation level as discussed in Section D), defining the 1-filter as treating X and Z errors separately is sufficient. This is because CNOT and CPHASE do not mix X and Z errors upon conjugation and the Hadamard transforms X errors to Z errors and vice versa.
- [A12] P. Aliferis and B. M. Terhal. Quantum Inf. Comp. 7, 139–157 (2007). arXive e-print quant-ph/0511065.